ASSESSMENT OF THE FLUX AND MONOCHROMATICITY CHARACTERISTICS OF A POLARIZED X-RAY SOURCE

by

Guili LIU [1,2]***, Siming GUO*** [2*]***, Zhen WANG*** [1,2]***, Wen LI*** [1,2]***, Derong DAI*** [1,2]***, Zhiwei LI*** [1,2]***, Dongjie HOU*** [2]***, Jinjie WU*** [2]***, Wanchang LAI*** [1]***, and Zhijun YANG*** [2*]

[1]Chengdu University of Technology, Chengdu, Sichuan Province, China
[2]National Institute of Metrology, Beijing, China

Scientific paper
https://doi.org/10.2298/NTRP2404251L

This paper presents an apparatus designed for the generation of polarized X-rays utilizing crystal Bragg diffraction techniques, which produces polarized X-rays energies within the range of 4-10 keV, facilitating the calibration of detection efficiency, energy resolution, polarization degree, and other parameters pertinent to polarized X-ray detectors. The apparatus comprises of a radiation source, a diffractive crystal, a rotating control mechanism, a detector and other components. High-precision generation of polarized X-rays can be achieved by diffracting through crystals with varying lattice constants at an angle of 45° using an X-ray tube and a Bragg diffraction apparatus. Monte Carlo simulations were conducted to evaluate air absorption effects on X-rays at varying energy levels, revealing an optimal measurement distance of 30 cm. Key metrics such as energy output, flux rate, energy resolution and monochromaticity for the generated polarized X-rays were evaluated through experimental measurements. The polarized X-ray flux rates were measured as: $4.135 \cdot 10^6$ $m^{-2}s^{-1}$ at 4.59 keV, $2.210 \cdot 10^7$ $m^{-2}s^{-1}$ at 6.39 keV, and $1.958 \cdot 10^7$ $m^{-2}s^{-1}$ at 10.029 keV. Monochromaticity values were: 1.48 % at 4.59 keV, 0.96 % at 6.39 keV, and 0.15 % at 10.029 keV. The apparatus is applicable to ground calibration of astronomical satellite payloads and detector development.

Key words: polarized X-ray, Bragg diffraction, monochromaticity, flux rate

INTRODUCTION

As a type of electromagnetic wave, X-rays exhibit polarization characteristics and play a crucial role in various fields, including astrophysics [1], nuclear physics research [2], and fluorescence imaging [3]. Consequently, polarized X-ray detection has garnered sustained interest in recent decades [4]. Scholars worldwide have conducted extensive investigations to advance this field. Polarized X-rays are employed to probe celestial structures, including low-frequency quasi-periodic oscillations [5], black hole spin dynamics [6], rotation direction predictions of isolated electromagnetic silent pulsars [7], high-energy polarized particle beams with elevated polarization levels [8], and so on. Energetic particles in the remnants of young supernovas and pulsar wind nebulae can produce X-rays by synchrotron radiation, thus measuring the polarization of this radiation aids in revealing magnetic field properties within particle acceleration regions, thereby facilitating studies on particle acceleration mechanisms [9]. The gas pixel detector (GPD) aboard China's Aurora Project satellite is capable of efficiently detecting photoelectrons on a 2-D plane, measuring X-ray polarization with high sensitivity, and monitoring variations in the pulsar's magnetic field through shifts in polarization [10]. China, Switzerland, Poland, and other nations collaborated to develop a specialized space detector for measuring the instantaneous radiation polarization of gamma-ray bursts: the gamma-ray polarization detector (POLAR). The Tiangong-2 spacecraft was equipped to perform high-precision polarization measurements of gamma-ray bursts within the 50-500 keV energy range, thereby constraining or validating models regarding the mechanisms behind gamma-ray bursts [11, 12]. A next-generation gamma-burst polarization detector (POLAR-2) is currently under development, with a planned launch around 2025. This will include the addition of a low-energy polarization detector (LPD), which will employ a gas-based polarization detection method for measuring the polarization of soft X-rays within the energy range of 2-10 keV [13, 14]. China's enhanced X-ray timing and polarimetry (eXTP) satellite, scheduled for launch in 2027, will

* Corresponding authors, e-mails: gsm@nim.ac.cn
yangzj@nim.ac.cn

carry four observational instruments. The polarization measuring X-ray focusing telescope array (PFA) is capable of detecting polarized X-rays within the energy range of 2-8 keV [15].

Prior to the deployment of the detector, ground-based polarization calibration is essential to quantify detector response amplitudes under linear polarized X-ray irradiation at varying energy levels. Recent studies have highlighted the influence of external radiation environments, such as solar flares, on beta radiation characteristics [16], this underscoring the necessity of stable and controllable, polarized X-ray sources for reliable calibration. Consequently, establishing a facility for the calibration of X-ray polarization is essential. Polarized X-rays can be generated through methods such as crystal diffraction, synchrotron radiation, inverse Compton scattering, and polarization converters. The predominant technique involves obtaining Monochromatic, linearly polarized X-rays via Bragg diffraction. As there are a few relevant calibration facilities in China, this study can supplement the lack of polarized X-ray generation facilities in China. In this study, we developed a crystal diffraction-based apparatus to generate and characterize polarized X-rays. By employing Bragg diffraction with X-rays produced by an optical machine on various crystals, we achieve a stable output of linearly polarized X-rays within the energy range of 4-10 keV. The apparatus's performance was systematically evaluated, encompassing parameters such as monochromaticity, energy resolution, detection efficiency, flux rate, among others. This study is of significant importance. Bragg diffraction provides a precise and stable method for generating polarized X-rays, addressing the limitations associated with the costly use of synchrotron radiation apparatuses that generate polarized X-rays. Through this research, professionals in related fields will gain access to a more economical apparatus for producing polarized X-rays, thereby facilitating accurate and reliable experimental data that can drive technological advancements in these domains.

THE THEORY OF CRYSTAL DIFFRACTION

The X-ray are fundamentally electromagnetic waves. During its propagation, the electric field vector $\vec{E}$ and the magnetic field intensity vector $\vec{H}$ oscillate perpendicularly and harmonically to each other, residing on a plane that is orthogonal to the direction of X-ray propagation, fig. 1 [17]. When the amplitudes of the electric and magnetic vectors are equal or when there exists a phase difference $\pm\pi/2$, and if the point vector rotates uniformly within the wave surface at an angular velocity ω, its trajectory describes a circle, resulting in circularly polarized X-rays. Conversely, when their amplitudes differ or when the phase difference deviates from $\pm\pi/2$, the path traced by this point vector becomes elliptical, characterizing elliptically polarized X-rays [18].

The X-rays exhibit wave-particle duality, when they interact with a crystal, each atom within the crystal acts as an independent X-ray source, maintaining the same wavelength as the incident X-ray. Due to the ordered arrangement of atoms in the crystal lattice, coherent X-rays reinforce one another in specific spatial directions while canceling out in others. This phenomenon, characterized by constructive interference of coherent X-rays along certain paths, is referred to as diffraction [17].

The Bragg's law

The X-rays are photons that exist within a specific wavelength range, and when they interact with the surface of a crystal, they induce Bragg diffraction, which adheres to Bragg's law [19]. The X-rays are diffracted by the crystal, fig. 2, and the diffraction direction of the first crystal face is oriented along path 1, while the diffraction direction of the second crystal face is aligned with path 2. The optical path difference between the diffraction lines of these two crystal planes is given by $\delta = l_1 - l_2$, where $l_2 = d/\sin\theta$, the $l_1 = l_2 \cos 2\theta$. For constructive interference to occur, this optical path difference must be an integer multiple of the incident X-ray wavelength, expressed as $\delta = n\lambda$ [20]. When the grazing angle of the X-ray incident on the crystal is varied by an angle θ, a corresponding change in the energy distribution of the X-rays occurs, as described by

$$2d\sin\theta = n\lambda \tag{1}$$

where d is the spacing between crystal planes, n – the order of diffraction and is an integer, and λ – the wavelength of X-rays. Provided that a specific angle is maintained, the X-ray from the continuous energy spectrum will yield a monochromatic X-ray of the corresponding wavelength following diffraction.

The Brewster's law

Following Bragg's law of X-ray diffraction, the intensity of the diffracted X-rays is dependent on the angle θ, and the integral reflection efficiency is defined as follows

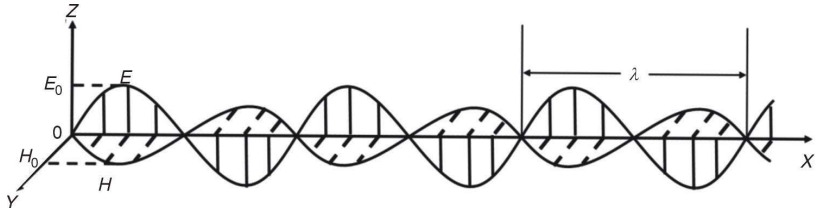

Figure 1. Schematic diagram of the simple harmonic motion of X-rays during propagation

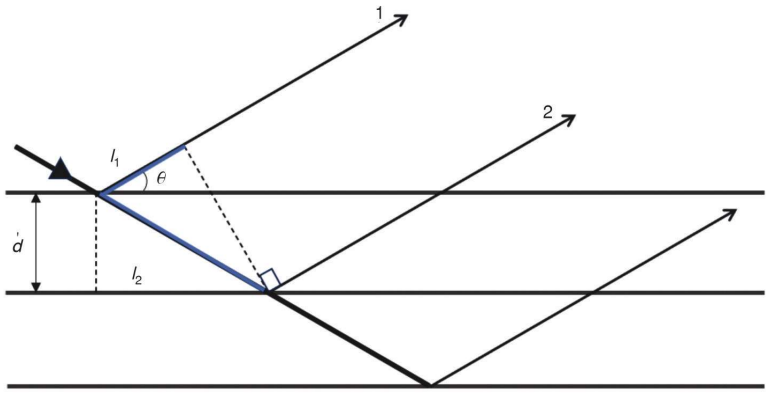

Figure 2. Schematic of crystal diffraction

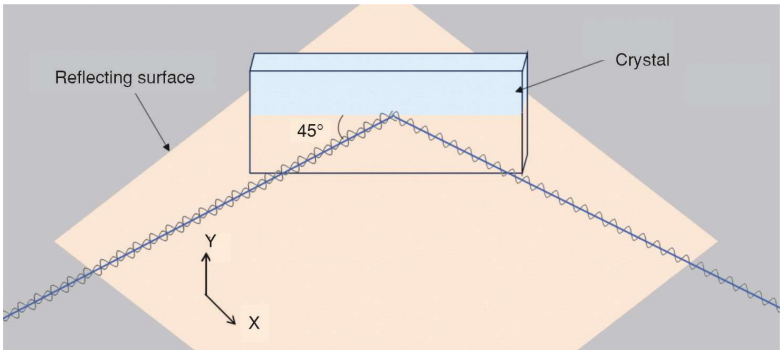

Figure 3. Polarization change of X-rays incident on a crystal at 45°, the outgoing X-rays retain only the y component perpendicular to the reflecting surface and therefore become linearly polarized

$$P_\lambda = \int_0^{\frac{\pi}{2}} P_\lambda(\theta)\mathrm{d}\theta \tag{2}$$

where P_λ is associated with the polarization direction of the incident X-ray, which can be categorized into parallel reflector orientation (z component) and perpendicular reflector orientation (y component) based on the surface of the reflector [21], as shown in fig. 3. Define the ratio k of reflectance

$$\mathrm{k} = \frac{P_\lambda^x}{P_\lambda^y} \tag{3}$$

The parameter k represents the ratio of the reflection efficiencies of the two components, and the polarization P can be articulated using the formula when k < 1

$$P = \frac{1-\mathrm{k}}{1+\mathrm{k}} \tag{4}$$

The reflection of photons at the interface between two distinct media adheres to Brewster's law

$$\theta_B = \arctan\frac{\mathrm{n}_2}{\mathrm{n}_1} \tag{5}$$

where n_1 and n_2 represent the refractive index of the two media, respectively. When photons propagate in a medium, the refractive index for different media satisfies the dispersion relation [22]

$$\mathrm{n} = 1 + \frac{\mathrm{N}e^2}{2\varepsilon_0 m}\frac{\omega_0^2 - \omega}{(\omega_0^2 - \omega^2)^2 + \omega^2\Gamma^2} \tag{6}$$

where m is the mass of the medium, N – the number density of particles, and Γ – the damping factor associated with electron vibrations. The intrinsic frequency of the medium is denoted as ω_0, while ω refers to the photon frequency, and ε_0 represents the vacuum's dielectric constant. In the case of X-rays, the wavelength of the photon is significantly shorter than that of visible light, which corresponds to a higher photon energy, the frequency is much larger than that of visible light, so the frequency can be considered to be close to infinity. At this time, whether air or crystal, the refractive index n is very close to 1, so the X-rays for each crystal Brewster angle are in the vicinity of 45 °. With this angle of incidence, in the eq. (4) the k = 0, in fig. 3, initially parallel to the reflecting surface of the x component in the reflection disappeared, and out of X-rays will only be retained perpendicular to the incident surface of the y component perpendicular to the incident plane, which is the linearly polarized X-ray [23].

CONSTRUCTION AND MEASUREMENT OF X-RAY POLARIZATION RADIATION APPARATUS

Introduction to the apparatus

The apparatus primarily consists of an X-ray tube, a high-voltage power supply controller, a turntable and a detector, along with other essential components, engineered to emit highly precise polarized X-rays within the energy range of 2-10 keV.

The X-ray tube is the core of the unit and produces low energy X-rays. The tube voltage range is 4-50 kV and the head current range is 0-1.5 mA. The X-ray tube's stainless-steel exterior incorporates a lead shielding layer, and internal insulation oil provides both cooling and high-voltage insulation. The beryllium window is filled with argon to prevent the absorption of X-rays by air, however, it also generates characteristic X-rays with an energy of approximately 3 keV. The X-ray tube is also equipped with water cooling to effectively reduce the tube temperature and improve the stability of the X-ray tube to ensure stable operation over long periods of time.

In this study, a high-purity germanium (HPGe) detector is employed. The effective detection volume of the HPGe detector is cylindrical in shape, with a bottom diameter of 11.1 mm and a length of 8.67 mm. The distance from the high-purity germanium to the beryllium window measures 2.25 mm, while the thickness of the beryllium window is 25 μm. The detection efficiency of the HPGe detector has been determined using Monte Carlo simulation software, fig. 4. Ten million X-ray photons were emitted at each energy point, and the simulation results were obtained by dividing the number of photons depositing energy within the detector by the number emitted [24].

Simulation of optical path and air absorption

When X-rays propagate through the atmosphere, their attenuation and scattering result from the absorption characteristics of air. To determine the optimal optical path length for generating polarized X-rays, open-source Monte Carlo software is employed to simulate X-ray absorption in the atmospheric medium [25]. In the modeling process, the detector is represented as a simplified cylinder, with the particle gun positioned directly in front of it to ensure that emitted particles enter the detector perpendicularly. The distance between the gun and the detector was then varied to 5 cm, 10 cm, 15 cm, 20 cm, 25 cm, 30 cm, 35 cm, 40 cm, 45 cm, 50 cm, 55 cm, and 60 cm to emit particles with energies ranging from 1 keV to 12 keV with an energy spacing of 1 keV. The quantity of particles emitted from a single energy source is 1 million. The final absorption of X-rays by air is the number of photons received by the detector divided by the number of photons emitted. Figure 5 presents the simulation results.

From the simulation results, when the distance is farther and the energy is lower, the attenuation and scattering of X-rays transmitted in the air are more severe, leading to stronger absorption. At energies close to 4 keV, most X-rays are absorbed by air, with transmittance dropping below 0.1 for distances beyond 40 cm. However, shorter distances (*e.g.*, 5-25 cm) introduce challenges in balancing crystal diffraction geometry and detector alignment due to spatial constraints.

Quantitative analysis of signal stability (SNR) reveals that the 30 cm optical path achieves optimal performance

$$\mathrm{SNR} = \frac{\mu}{\sigma} \tag{7}$$

where μ is the mean transmittance values and σ – the standard deviation, the results presented in tab. 1.

At 30 cm, the air transmittance for 4 keV exceeds 0.1 (0.0475), which satisfies the minimum flux threshold for generating polarized X-rays. Concurrently, this distance provides the highest SNR (2.04) across all tested configurations, indicating superior stability with minimal signal fluctuations. The SNR advantage arises from two factors:

– Attenuation-noise trade-off: longer paths (>30 cm) reduce signal intensity (*e.g.*, 60 cm: μ = 0.322), while shorter paths (<30 cm) amplify noise from air scattering (*e.g.*, 5 cm: σ = 0.367).

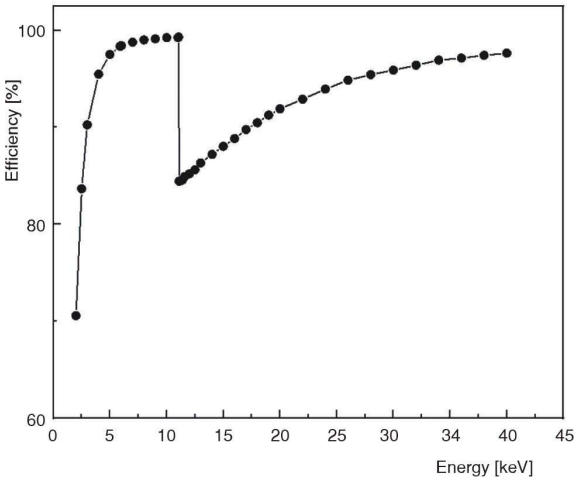

Figure 4. Results of simulations regarding the detection efficiency of HPGe

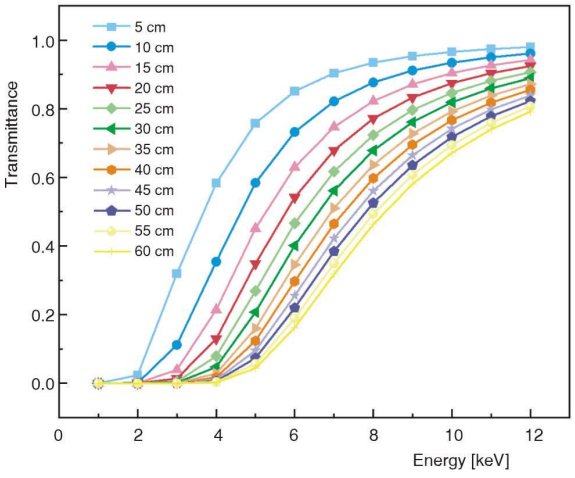

Figure 5. Results of simulated air absorption analysis

Table 1. The SNR analysis of X-ray transmittance at varying distances

Distance [cm]	μ	σ	SNR
5	0.616	0.367	1.68
10	0.613	0.329	1.86
15	0.599	0.306	1.95
20	0.578	0.289	2.00
25	0.550	0.272	2.02
30	0.521	0.256	2.04
35	0.490	0.242	2.03
40	0.457	0.228	2.00
45	0.423	0.214	1.98
50	0.388	0.201	1.93
55	0.354	0.187	1.89
60	0.322	0.174	1.85

– Crystal geometry constraints: the 30 cm length accommodates Bragg diffraction alignment (45° angle for LiF200 crystal) and minimizes edge diffraction artifacts.

Thus, the 30 cm optical path is selected as the optimal balance between polarized X-ray yield (transmittance >0.1 at 4 keV) and operational robustness (SNR >2.0).

Polarizing X-ray apparatus

A rotating platform has been engineered for the precise positioning of the X-ray tube and crystal. Both the X-ray tube and crystal are aligned along a common horizontal axis, with the angle between the crystal and optical apparatus adjustable via a rotating support mechanism. When the optical apparatus is rotated by 90°, the angle of incidence at the crystal is set to 45°, resulting in an orthogonal relationship (90°) between the incoming and outgoing X-ray paths through the crystal, thereby facilitating polarized X-ray generation. A HPGe is subsequently positioned in line with the exit direction of the crystal. Given that we have allocated a total optical path length of 30 cm, both distances from their respective centers-the X-ray tube to crystal center and HPGe to crystal center-are established at 15 cm each. Following this configuration, assembly of the polarized X-ray generation apparatus can commence as illustrated in the accompanying diagram, fig. 6.

Diffraction-patterned crystal

Given that the energy range of detectors employed for detecting polarized X-rays in the current space exploration program spans from 2-10 keV, it can be inferred from the calculations based on eq. (1) that the Bragg diffraction energies of numerous Bragg crystals at an angle of 45° fall within this range. Furthermore, by utilizing a polarized X-ray apparatus,

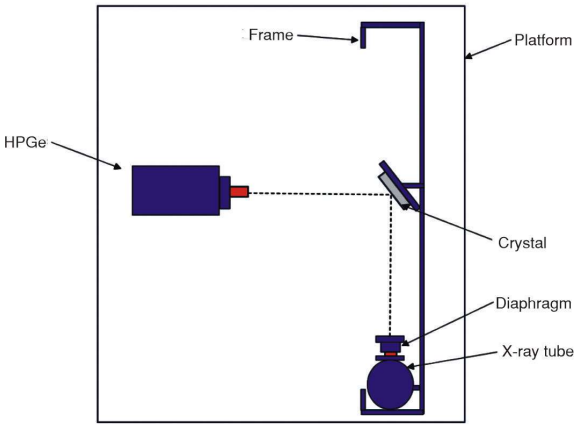

Figure 6. Schematic representation of a polarizing X-ray apparatus

one can ascertain both the polarization energy and counting rates associated with various crystals. Concurrently, the theoretical values for crystal lattice spacing are computed according to [26]

$$d = \frac{a}{\sqrt{h^2 + k^2 + l^2}} \tag{8}$$

where d is the spacing between crystal faces, a – the lattice constant, and h, k, l are the Miller indexes, of a crystal plane which should be referenced against the three numerical values following the crystal name in tab. 2.

In the course of the experiment, a diaphragm with a thickness of 4 mm was positioned at the X-ray tube port. The tube voltage was calibrated to 10 kV, while the tube current was maintained at 0.2 mA, ensuring that the dead time remained within 3 %. This configuration guarantees the reliability of detector measurements. Nevertheless, the polarization peak is not observable when measuring LiF420 under these conditions, as the energy of the continuous spectrum of X-rays, generated by bremsstrahlung at 10 kV, predominantly resides within the 6-8 keV range, while the number of X-ray photons at an energy of 9.7 keV remains exceedingly low. Therefore, the tube voltage of the X-ray tube was adjusted upward to 15 kV during the measurement of LiF420, and the data in tab. 1 were obtained after re-measurement.

Table 2. Crystal spacing and detector measurement results

Crystallography	d [Å^{-1}]*	Energy [keV]	Count rate [cps]	Dead time [%]
LiF420	0.900	9.9	1033.9	2.69
LiF220	1.423	6.3	1064.23	2.68
LiF200	2.013	4.5	400.15	2.72
PET	4.870	4.0	14.00	0.43
ADP	5.324	4.9	40.95	0.46
XS-55	27.500	6.4	165.37	0.46

* 1Å = $1 \cdot 10^{-10}$ m

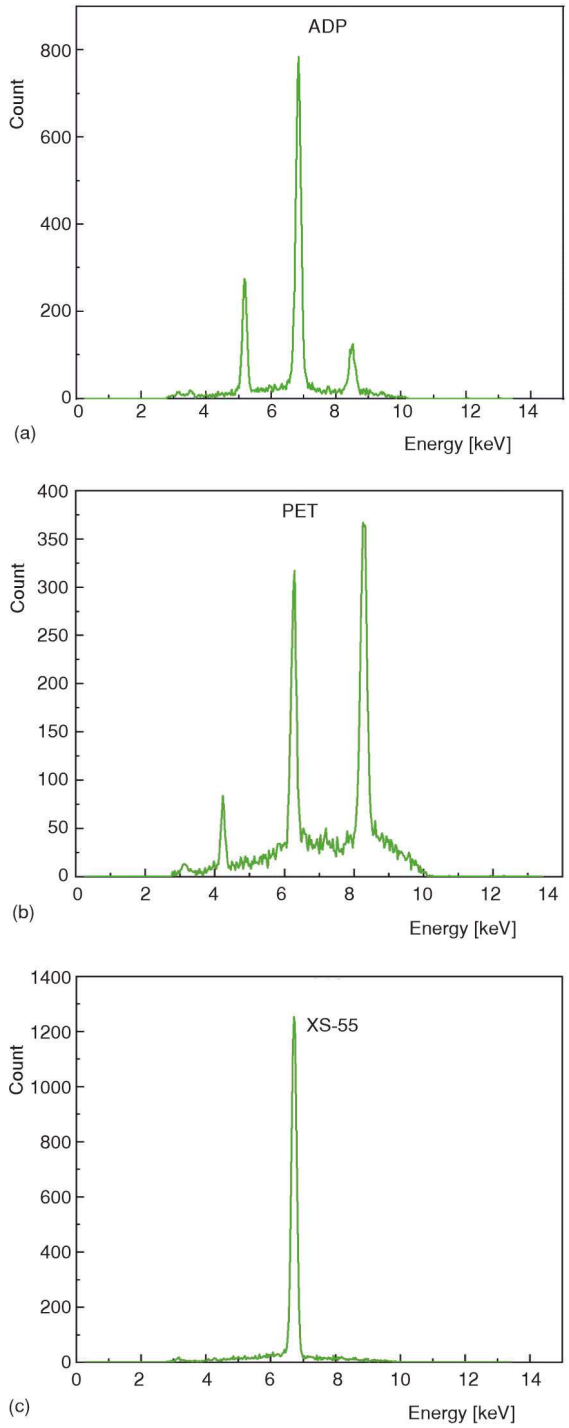

Figure 7. Partial energy spectrum obtained from the crystal deflection experiment

From tab. 1, pentaerythritol (C5H12O4, PET) and ammonium dihydrogen phosphate (NH4H2PO4, ADP), when formed into organic multilayer crystals, exhibit a significant crystal face spacing. Consequently, the detector does not register their primary diffraction peak but rather higher-order harmonics. This results in multiple peaks observable in the energy spectrum, as illustrated in fig. 7. Therefore, these two crystals are deemed unsuitable for this specific energy segment of polarizing crystals. The XS-55 is a multilayer film composed of two distinct inorganic materials, such as silicon and tungsten, arranged in an alternating manner. The spacing between the crystal surfaces exceeds that of organic compounds. Given that its theoretical first-order diffraction energy at a 45° angle is merely 0.16 keV, the energy values presented in tab. 1 are likely influenced by higher harmonics beyond grade 20. While the count appears satisfactory, the purity of the energy spectrum remains inadequate, rendering it unsuitable for use as a polarizing crystal within this energy range. The small interfacial spacing and elevated count rate of LiF crystals suggest that the conditions for polarization are more readily achievable, resulting in stronger and clearer polarization peaks that facilitate detection. This indicates that these crystals are advantageous for the generation of polarized X-rays. Therefore, after comprehensive consideration, we have selected three types of LiF crystals-LiF420, LiF220, and LiF200-as our final polarizing materials.

RESULTS AND DISCUSSION ON POLARIZATION MEASUREMENT

To assess the apparatus's performance, a systematic evaluation and analysis of its energy spectrum data, energy resolution, flux rate, and monochromaticity were conducted.

Measurements of the energy spectrum

The polarization X-ray energy spectrum data acquired from the HPGe detector were analyzed and visualized using Origin software. When polarizing X-rays are generated through crystal diffraction, the resulting monochromatic X-rays simultaneously adhere to Bragg's law, leading to the emergence of distinct monochromatic peaks in the energy spectrum at an incident angle of 45° on the crystal. The fig. 8 illustrates the energy spectrum recorded by the detector when X-rays penetrate the crystal at an incidence angle of 45°, utilizing stop sizes of 2 mm, 4 mm, and 6 mm in their original positions. For LiF220, The polarization peak energy was 6.39 keV with a 2 mm diaphragm, with up to 54 309 counts in one minute, with an energy resolution of 2.90 %, and 128 331 counts in one minute were measured at 4 mm diaphragm without any other changes in the measurement setup, which is an increase in counts compared to the 2 mm diaphragm, with an energy resolution of 2.75 %; when measured with a 6 mm diaphragm, 130 087 counts were obtained in one minute, which is not much different from the 4 mm counts. The count of LiF200 per minute is lower than that of LiF220, which exhibits double peaks and undergoes two diffraction events. The energy resolution under three distinct stop conditions is approximately 3.33 %. In contrast, the counts

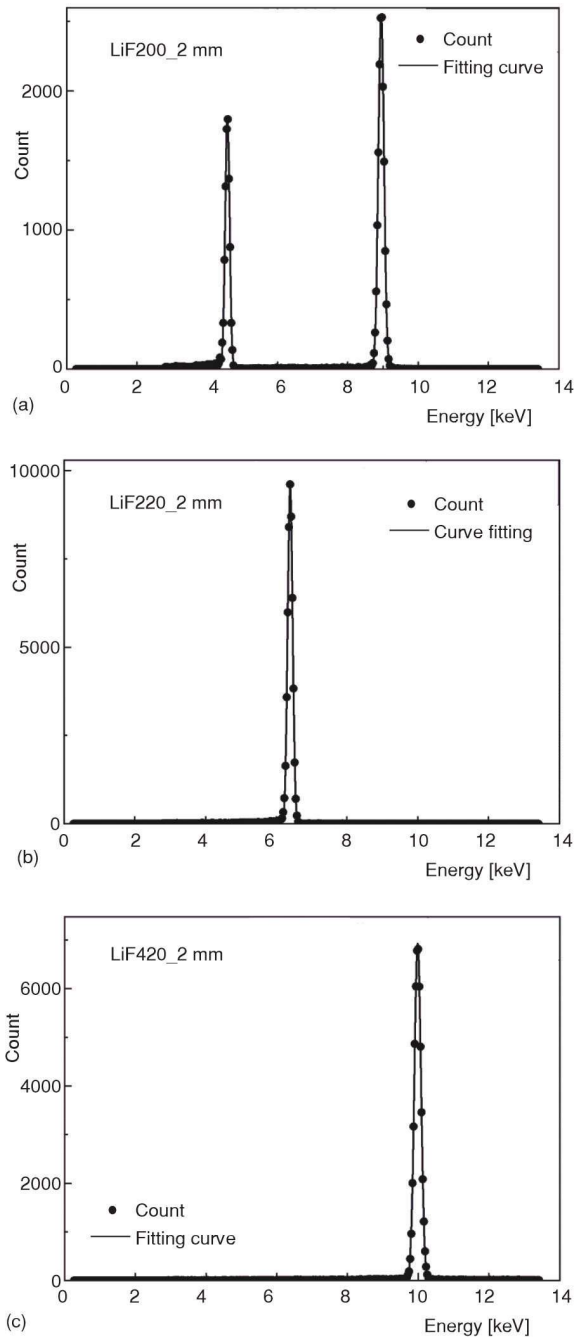

Figure 8. The Energy spectra of LiF200 (a), LiF220 (b), LiF420 (c) measured by HPGe at an aperture of 2 mm

for LiF420 and LiF220 in one-minute show minimal variation, with the energy resolution across these three different stop conditions being around 2.57 %.

Measurement of flux rates

Analyzing the flux rate of polarized X-rays is essential for assessing the performance of polarized X-ray apparatus, specifically, it allows for a comprehensive understanding of the transmission efficiency for polarized X-rays, which is crucial in determining both the sensitivity and detection capabilities of these apparatuses. In this experiment, a HPGe detector was employed to quantify the counts of omnipresent peaks from polarized X-rays across various crystal substrates. The flux rate Φ of polarized X-rays is defined as the number of polarized photons traversing a unit area per unit time, and its relationship can be expressed as follows [27]

$$\Phi = \frac{\mathrm{N}}{At} \tag{9}$$

where N is the number of counts of the overall peaks of polarized X-rays measured by the detector, A – the bottom area of the effective detection volume of the HPGe, and t – the measurement time.

In order to evaluate the flux rate of the apparatus, this study used a high-purity germanium detector to measure the all-around peak counts of polarized X-rays at energies of 4.59 keV, 6.39 keV, and 10.029 keV produced by LiF200, LiF220, and LiF420 crystals at 2 mm, 4 mm, and 6 mm diaphragms, for 60 seconds. By integrating eq. (9), the flux rate of the polarization apparatus across various crystal types and stop configurations is computed. In order to evaluate the reliability of the flux rate, we also calculate the relative deviation

$$\varepsilon_{\Phi} = \frac{\sigma_{\Phi}}{\Phi} = \frac{\sigma_{\mathrm{N}}}{\mathrm{N}} = \frac{\sqrt{\mathrm{N}}}{\mathrm{N}} = \frac{1}{\sqrt{\mathrm{N}}} \tag{10}$$

The results presented in tab. 3.

The results of the calculations indicate that the apparatus exhibits a flux rate of $4.135 \cdot 10^6$ $m^{-2}s^{-1}$ at an energy level of 4.59 keV with a diaphragm size of 4 mm, while at an energy level of 6.39 keV and the same dia-

Table 3. The results of calculations regarding the monochromaticity of polarized X-rays

Crystallography	Diaphragm [mm]	Energy [keV]	N	Φ [$m^{-2}s^{-1}$]	ε_{Φ} [%]	$\Phi \pm \Delta\Phi$ [$m^{-2}s^{-1}$]
LiF200	2	4.59	10153	$1.749 \cdot 10^6$	1.0	$(1.749 \pm 0.017) \cdot 10^6$
	4		24009	$4.135 \cdot 10^6$	0.6	$(4.135 \pm 0.026) \cdot 10^6$
	6		24988	$4.304 \cdot 10^6$	0.6	$(4.135 \pm 0.026) \cdot 10^6$
LiF220	2	6.39	54309	$9.354 \cdot 10^6$	0.4	$(4.135 \pm 0.026) \cdot 10^6$
	4		128331	$2.210 \cdot 10^7$	0.3	$(2.210 \pm 0.006) \cdot 10^7$
	6		130087	$2.241 \cdot 10^7$	0.3	$(2.241 \pm 0.006) \cdot 10^7$
LiF420	2	10.029	52582	$9.056 \cdot 10^6$	0.4	$(9.056 \pm 0.040) \cdot 10^6$
	4		113662	$1.958 \cdot 10^7$	0.3	$(1.958 \pm 0.006) \cdot 10^7$
	6		128954	$2.221 \cdot 10^7$	0.3	$(2.221 \pm 0.006) \cdot 10^7$

phragm size, the flux rate increases to $2.2^{10}\cdot10^7$ $m^{-2}s^{-1}$. Furthermore, at an energy level of 10.029 keV with a diaphragm aperture of 4 mm, the flux rate measured is $1.958\cdot10^7$ $m^{-2}s^{-1}$. Throughout the energy range from (4-10) keV, all the recorded flux rates fall between $1.749\cdot10^6$ $m^{-2}s^{-1}$ ~$2.241\cdot10^7$ $m^{-2}s^{-1}$, and the relative deviation is less than 1 %, demonstrating that the apparatus maintains high flux output and efficiency across various energy levels, thereby facilitating more precise and repeatable polarization X-ray experiments which are beneficial for calibrating polarization X-ray detectors.

Investigation of monochromaticity

Monochromaticity serves as a critical metric for assessing the performance of polarized X-ray apparatuses, reflecting the apparatus's capability to generate pure polarized X-rays and thereby evaluating the concentration of its energy distribution [28]. In the experiment, the HPGe detector is employed to assess the energy resolution of the all-purpose peak of polarized X-rays across various crystal substrates. After accounting for the intrinsic energy resolution of the HPGe detector, we derive the monochromatic characteristics of the polarized X-ray produced by this apparatus. The relationship between the monochromaticity and the energy resolution of the detector and the energy resolution of the measured energy spectrum is shown in

$$\delta_1^2 + \delta_2^2 = \delta_3^2 \tag{11}$$

where δ_1 is the intrinsic energy resolution of the HPGe detector, and δ_2 – the monochromaticity of the radiation source, and δ_3 – the energy resolution as measured by the detector itself. The intrinsic energy resolution δ_1 of HPGe can be determined through calibration with a radioactive source, which is generally accepted to produce unbroadened radiation. Table 4 presents the data utilized for calibrating the energy resolution of HPGe using radioactive sources

The relationship between the detector's energy resolution and intrinsic energy is illustrated in [29]

$$\delta_1 = \frac{a + b\sqrt{E + cE^2}}{E}\cdot 100\,[\%] \tag{12}$$

where E is the energy of the radioactive source, a, b, and c are the calibrated parameters, The values for energy and energy resolution presented in tab. 3 are derived from fitting based on

Table 4. Calibration of high purity germanium detectors using radioactive sources

Nuclide	E [keV]	FWHM [keV]	δ_1 [%]
^{55}Fe	5.899	0.183	3.102
^{57}Co	6.404	0.176	2.748
^{109}Cd	22.163	0.332	1.498
^{241}Am	59.541	0.347	0.583
^{133}Ba	80.767	0.393	0.487
^{152}Eu	121.436	0.468	0.385

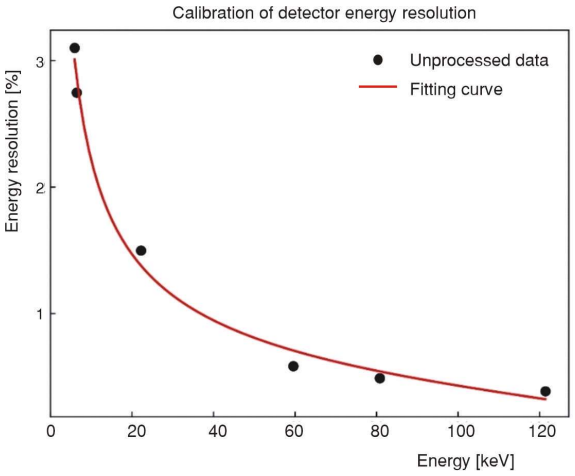

Figure 9. Calibration of detector energy resolution

$$\delta_1 = \frac{0.02452 + 0.06416\sqrt{E - 0.006E^2}}{E}\cdot 100\,[\%] \tag{13}$$

The actual energy resolution δ_3, as measured by the detector, is correlated with both the half-height width and the energy of the universal peak; the precise relationship is delineated in

$$\delta_3 = \frac{FWHM}{E}\cdot 100\,[\%] \tag{14}$$

To assess the monochromaticity of the apparatus, we measured the energy resolution of polarized X-rays generated by LiF200, LiF220, and LiF420 crystals with diaphragm sizes of 2 mm, 4 mm, and 6 mm using a high-purity germanium detector. By integrating eqs. (11), (13), and (14), we calculated both the intrinsic energy resolution of the detector and the energy resolution as measured by it, thereby elucidating the monochromatic characteristics of the polarized X-ray produced by the apparatus. The results of these calculations are presented in tab. 5.

Calculated results show that the monochromaticity of the apparatus is 1.48 % at 4.59 keV energy with a 4 mm diaphragm, 0.96 % at 6.39 keV energy with a 4 mm diaphragm, and 0.15 % at 10.029 keV energy with a 4 mm diaphragm. The monochromatism within the energy range of 4-10 keV is less than 1.48 %, thereby offering enhanced accuracy in polarization X-ray energy information for the calibration of polarization detectors and improving the overall calibration precision of these instruments.

CONCLUSION

We designed and implemented an apparatus for generating polarized X-rays via crystal diffraction, followed by performance evaluation. This apparatus reliably produces linearly polarized X-rays within the

Table 5. Polarized X-ray monochromaticity calculation results

Crystallography	Diaphragm [mm]	*E* [keV]	FWHM [keV]	δ_1 [%]	δ_3 [%]	δ_2 [%]
LiF200	2	4.590	0.150	3.27	3.49	1.22
	4		0.145	3.16		1.48
	6		0.156	3.40		0.78
LiF220	2	6.390	0.162	2.54	2.87	1.35
	4		0.173	2.71		0.96
	6		0.174	2.72		0.92
LiF420	2	10.029	0.219	2.18	2.21	0.33
	4		0.221	2.20		0.15
	6		0.221	2.20		0.15

energy range of 4-10 keV, thereby offering a more precise and stable source for the calibration of polarized X-rays. In contrast to the costly synchrotron radiation apparatus, this apparatus offers advantages such as affordability and ease of operation, thereby presenting a more economical option for research in related fields. Through experiments and simulations, three kinds of crystals, LiF420, LiF220 and LiF200, with small crystal plane spacing and elevated count rate, are identified as polarizing crystals, which can effectively produce polarized X-rays with monochromaticity better than 1.48 % and fluxes ranging from $1.749 \cdot 10^6$-$2.241 \cdot 10^7$ $m^{-2}s^{-1}$, with high energy resolution and high fluxes, and can effectively inhibit the interference of background noise, thus providing a reliable source for related research. The apparatus is applicable in fields such as astrophysics, nuclear physics research, and fluorescence imaging, thereby advancing the calibration technology for polarization X detectors. Future optimizations of the apparatus's design will improve performance, stability, and applicability to broader energy ranges.

ACKNOWLEDGMENT

We would like to express our gratitude to the staff of National Institute of Metrology of China (NIM), who have provided invaluable assistance during the development phase of our project. We wish to acknowledge the support of the following project funds from NIM: 2023YFC2206502, 12205289, and AKYZD2412. We declare that we have no known competing financial interests or personal relationships that could have appeared to influence the work reported in this paper. We appreciate the contributions of these funds, which have been instrumental in the successful completion of our research.

AUTHORS' CONTRIBUTIONS

The manuscript is written by G. Liu and Z. Wang and discussion by S. Guo, W. Li, D. Dai, Z. Li, D. Hou, J. Wu, W. Lai, and Z. Yang. All authors participated in the preparation of the final version of the manuscript.

ORCID NO

G. Liu: 0009-0003-4090-2770

REFERENCES

[1] Chattopadhyay, T., Hard X-Ray Polarimetry-An Overview of the Method, Science Drivers, and Recent Findings, *Journal of Astrophysics and Astronomy, 42* (2021), 2, 106
[2] Renzhou, Z., *et al.*, Simulation of Polarimetric Photoelectric Process in X-Ray Polarization Detector (in Chinese), *Acta Optica Sinica, 44* (2024), 3, pp. 329-336
[3] Wu, C., Li, L., First Demonstration of Compton Camera Used for X-Ray Fluorescence Imaging, *IEEE Transactions on Medical Imaging, 42* (2023), 5, pp. 1314-1324
[4] Yue, M., *Polarization Characteristics and CT Imaging Applications of All-Optical Inverse Compton Scattering*, Tsinghua University, 2020
[5] Giacconi, R., *et al*., Evidence for X-Rays from Sources Outside the Solar System, *Phys. Rev. Let, 9* (1962), 11, pp. 439-443
[6] Qin, Y., *et al*., Hypercritical Accretion for Black Hole High Spin in Cygnus X-1, *Research in Astronomy and Astrophysics, 22* (2022), 3, 6
[7] Soffitta, P., *et al*., A Polarized View of the Hot and Violent Universe, *Experimental Astronomy, 51* (2021), 3, pp. 1109-1141
[8] Ting, S., *et al*., Review on Laser-Driven High-Energy Polarized Electron and Positron Beams and G-Rays, *Acta Physica Sinica, 70* (2021), 8, 12
[9] Tianxian, N., Ping, Z., X-Ray Polarization Imaging of Supernova Remnants and Pulsar Wind Nebulae, *Progress in Astronomy, 42* (2024), 1, pp. 76-85
[10] ***, Department of Engineering Physics and Center for Astrophysics T U. PolarLight: a CubeSat X-Ray Polarimeter Based on the Gas Pixel Detector[J], *Experimental Astronomy, 47* (2019), 1-2, pp. 225-243
[11] Produit, N., *et al*., Design and Construction of the POLAR Detector, *Nuclear Inst. and Methods in Physics Research, A, 877* (2017), 1, pp. 259-268
[12] Jianchao, S., *et al*., Research Progress on Polarization Measurements of Gamma-Ray Burst Prompt Emissions and the Test of Pulsar Navigation with POLAR, *Chinese Science Bulletin, 68* (2023), 22, pp. 2951-2960
[13] Feng, Z. K., *et al*., In-Orbit Background and Sky Survey Simulation Study of POLAR-2/LPD, *The Astrophysical Journal, 960* (2024), 1, pp. 13-87
[14] Xie, Y., Development and Performance Testing of the Ground Calibration Platform for the Polar-2, Guangxi University, 2023

[15] Yupeng, X., *et al*., Explore Extreme Universes – from HXMT to eXTP and HERD, *Modern Physics, 33* (2021), 2, pp. 12-21
[16] Peleg, Y., Orion, I., The Impact of Strong Solar Flares on Thorium Beta Radiation Count-Rate, *Nucl Technol Radiat, 38* (2023), 2, pp. 102-107
[17] ***, Society E H T S, Al E B W C, Structural Analysis of Metals[G]. Beijing, China: China Machine Press, 1989
[18] Kaihua, Z., New Concept Physics Tutorial, Optics (in Chinese)[M], New Concept Physics Tutorial, Optics, 2004
[19] Aristov, V. V., *et al*., Observation of X-Ray Bragg Diffraction on the Periodic Surface Relief of a Perfect Silicon Crystal, *Optics Communications, 58* (1986), 5, pp. 300-302
[20] Bingxin, H., Wenjiang, Q., Using the Variable Separation Method to Solve Axisymmetric Magnetic Field in Equilibrium States, *College Physics, 42* (2023), 4, pp. 4-12
[21] Henke, B. L., *et al*., X-Ray Interactions: Photoabsorption, Scattering, Transmission, and Reflection at E = 50-30,000 eV, Z = 1-92, *Atomic Data & Nuclear Data Tables, 54* (1993), 2, pp. 113112-113306
[22] Zangwill, A., Modern Electrodynamics: Cambridge University Press, 2012
[23] Fabio, M., *et al*., A Very Compact Polarizer for an X-Ray Polarimeter Calibration[J], *UV, X-Ray, and Gamma-Ray Space Instrumentation for Astronomy XV, 6686* (2007), 1, pp. 668610-668610-12
[24] Haiqing, Z., *et al*., The Determination of Functional Relationship Between Point Source Efficiency and its Space Position for an HPGe Detector[J], *Nuclear Techniques, 33* (2010), 11, pp. 839-843
[25] Kai, H., *et al*., A Brief Discussion on the Application of Monte Carlo Algorithm in the Study of X-Ray Characteristics, *Science and Technology Innovation Herald, 16* (2019), 7, 2
[26] Sardela, M. R., *X-Ray Diffraction and Reflectivity*, (M. Sardela, Ed. Springer, New York, USA, 2014, pp. 1-41
[27] Hua-Peng, L., *et al*., Absolute Measurement of Photon Flux for Synchrotron Radiation Hard X-Rays, *Optics and Precision Engineering, 25* (2017), pp. 2845-2851
[28] Siming, G., *et al*., Design and Monochromaticity of a Monochromatic X-Ray Calibration Device, *Acta Metrologica Sinca, 39* (2018), B12, 5
[29] Fulong, L., *et al*., A Wavelet Denoising Method for Gamma SpectrometryAnalysis Based on MATLAB GUI, *Nuclear Eleetronies & Detection Technology, 33* (2013), 10, pp. 1266-1270

Received on January 12, 2025
Accepted on March 10, 2025

Гуејли ЉУ, Симинг ГУО, Џен ВАНГ, Вен ЛИ, Дежунг ДАЈ, Цивеј ЛИ, Дунгђе ХОУ, Ђинђе ВУ, Ванчанг ЛАЈ, Џиђуен ЈАНГ

ПРОЦЕНА КАРАКТЕРИСТИКА ФЛУКСА И МОНОХРОМНОСТИ ПОЛАРИЗОВАНОГ ИЗВОРА РЕНДГЕНСКОГ ЗРАЧЕЊА

Представљен је апарат пројектован за генерисање поларизованих рендгенских зрака употребом технике кристалне Брагове дифракције, која производи енергију поларизованих рендгенских зрака у опсегу 4-10 keV, олакшавајући калибрацију ефикасности детекције, енергетске резолуције, степена поларизације и других параметара који се односе на детекторе поларизованих рендгенских зрака. Апарат се састоји од извора зрачења, дифракционог кристала, ротационог контролног механизма, детектора и других компоненти. Генерисање поларизованих рендгенских зрака високе прецизности може се постићи дифракцијом кроз кристале са различитим константама решетке под углом од 45° коришћењем рендгенске цеви и Браговог дифракционог апарата. Монте Карло симулације спроведене су да би се проценили ефекти апсорпције ваздуха на рендгенске зраке на различитим нивоима енергије, откривајући оптимално растојање мерење од 30 cm. Кључни подаци као што су излазна енергија, јачина флукса, енергетска резолуција и монохромност за генерисане поларизоване рендгенске зраке процењени су експерименталним мерењима. Јачина поларизованог флукса рендгенских зрака измерене су као: $4.135 \cdot 10^6$ m^{-2}s^{-1} на 4.59 keV, $2.210 \cdot 10^7$ m^{-2}s^{-1} на 6.39 keV и $1.958 \cdot 10^7$ m^{-2}s^{-1} на 10.029 keV. Вредности монохромности биле су: 1.48 % на 4.59 keV, 0.96 % на 6.39 keV и 0.15 % на 10.029 keV. Апарат је погодан за калибрацију на тлу, да одговара носивости астрономских сателита и за развој детектора.

Кључне речи: поларизовано рендгенско зрачење, Брагова дифракција, монохромност, јачина флукса